Journal of Marine Research, 74, 71–99, 2016

Western North Pacific Integrated Physical-Biogeochemical Ocean Observation Experiment (INBOX): Part 2. Biogeochemical responses to eddies and typhoons revealed from the S1 mooring and shipboard measurements

by Ryuichiro Inoue[1,2], Makio C. Honda[3], Tetsuichi Fujiki[1], Kazuhiko Matsumoto[3], Shinya Kouketsu[1], Toshio Suga[1,4], and Toshiro Saino[5]

ABSTRACT

An interdisciplinary project called S1-INBOX (Western North Pacific Integrated Physical-Biogeochemical Ocean Observation Experiment conducted around the S1 biogeochemical mooring site) was carried out during the summer of 2011 in the oligotrophic, subtropical North Pacific Ocean near biogeochemical mooring S1 (30° N, 145° E). Results from the S1 mooring during S1-INBOX revealed a large export flux at a depth of 200 m, a high chlorophyll *a* concentration in the deep chlorophyll maximum layer, and a high potential photochemical efficiency of photosystem II. These phenomena were associated with vertical uplift of isopycnal surfaces at the edge of a cyclonic eddy and a transition from the cyclonic eddy to an anticyclonic eddy. Shipboard biogeochemical surveys conducted during oligotrophic conditions in July 2011 revealed that the phytoplankton community in these waters was dominated by small species that are responsive to intermittent supplies of nutrients. Surface wind forcing because of Typhoons MA-ON and SONCA may have generated near-inertial oscillations. Diapycnal mixing associated with near-inertial waves was also related to high export fluxes, the indication being that propagation of near-inertial internal waves and subsequent mixing may have been important to biogeochemical phenomena during S1-INBOX.

Keywords: Cyclonic eddy, typhoon, phytoplankton, nutrient, export flux, mooring, shipboard sampling

1. Research and Development Center for Global Change, Japan Agency for Marine-Earth Science and Technology (JAMSTEC), 2-15 Natsushima-cho, Yokosuka 237-0061, Japan.
2. Corresponding author: ***e-mail: rinoue@jamstec.go.jp***
3. Department of Environmental Geochemical Cycle Research, Japan Agency for Marine-Earth Science and Technology (JAMSTEC), 2-15 Natsushima-cho, Yokosuka 237-0061, Japan.
4. Department of Geophysics, Graduate School of Science, Tohoku University, 6-3 Aramaki-Aza-Aoba, Aoba-ku, Sendai, 980-8578, Japan.
5. Deceased.

1. Introduction

Oligotrophic conditions in subtropical gyres confound quantification of global net community production in terms of oxygen production and carbon fixation. Hence, there have been efforts to quantify the mechanisms that supply nutrients to the euphotic zone (Jenkins and Goldman 1985; Jenkins 1988; Spitzer and Jenkins 1989; Michaels et al. 1994; McGillicuddy et al. 1998). The goal of the Western North Pacific Integrated Physical-Biogeochemical Ocean Observation Experiment (INBOX) was to use an array of dissolved oxygen (DO) floats to observe the evolution of the temporal and spatial relationships during the summer between biogeochemical phenomena and physical processes, such as westward-propagating eddies and atmospheric disturbances.

S1-INBOX observations were carried out near biogeochemical mooring S1 (30° N, 145° E) beginning in July 2011. Site S1 was located near the southern edge of the Kuroshio recirculation gyre (Fig. 1). The mixed-layer depth clearly varies seasonally at S1, and the winter mixed layer can reach the depth of subtropical mode water. Several mesoscale eddies and typhoons passed near the S1 mooring site every year (Inoue and Kouketsu 2016). Both processes could modify stratification at the base of the euphotic zone in summer and therefore bring up nutrient-rich water into the euphotic zone (e.g., McGillicuddy et al. 2007; Lin 2012).

The recent, in situ EDDIES experiment in the oligotrophic subtropics of the North Atlantic revealed the effects of different types of eddies on biogeochemical phenomena (e.g., Benitez-Nelson and McGillicuddy 2008). A high concentration of diatoms (*Chaetoceros* and *Rizosolenia*) was observed at the center of an anticyclonic mode water eddy (Bibby et al. 2008), and it was proposed that this high biomass was maintained by eddy-Ekman pumping (McGillicuddy et al. 2007; McGillicuddy, Ledwell, and Anderson 2008). In contrast, in a decaying cyclonic eddy and at the periphery of eddies, nano- and picophytoplankton (*Prochlorococcus*, *Synechococcus*, pelagophytes, and prymnesiophytes) typically dominate the phytoplankton community in the deep chlorophyll maximum (DCM) during the summer (Bibby et al. 2008). Because differences in phytoplankton composition between eddies could influence biogeochemical processes and food web dynamics, it was also important to identify the dominant species during the S1-INBOX and to relate phytoplankton community composition to physical oceanographic conditions.

Tropical cyclones and storms are also known to enhance phytoplankton productivity (e.g., Lin et al. 2003; Shibano et al. 2011; Lin 2012; Zhao et al. 2015). Enhancement could occur as a result of strong wind forcing, and it is important to note that the physical response of the ocean can differ between the forced and relaxation stages (e.g., Price 1981, 1983; Price, Sanford, and Forristall 1994). During the forced stage, mixed-layer deepening and Ekman pumping are important to the processes of entrainment and upwelling, respectively. Those processes can bring relatively deep water into the surface mixed layer. During the relaxation stage, near-inertial oscillations can further deepen the mixed layer via shear instability at the base of the mixed layer. Some of the oscillations in the mixed layer can propagate

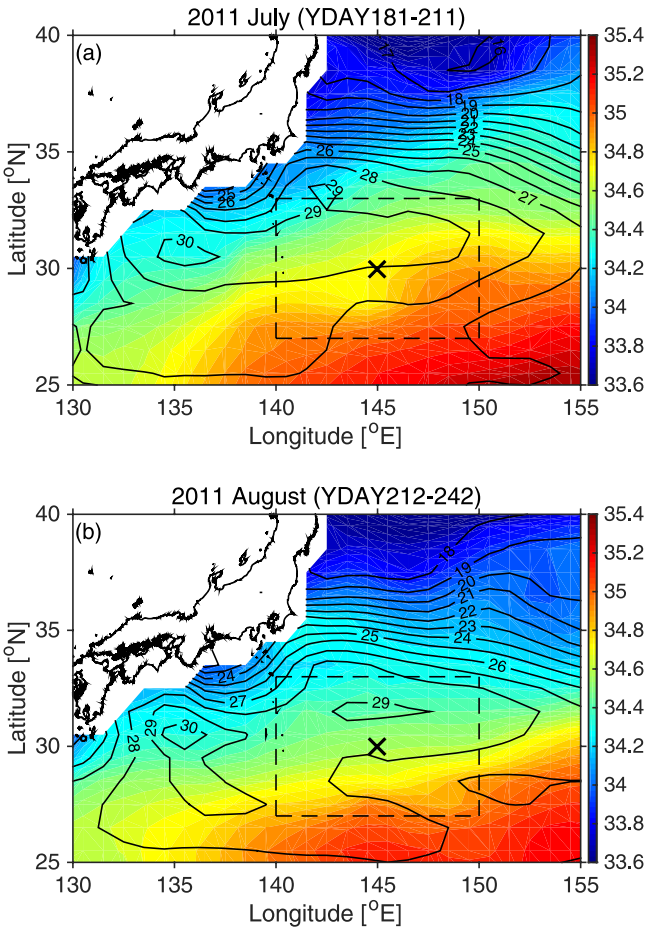

Figure 1. Horizontal map of the monthly averaged salinity and geopotential (black contour, $m^2\ s^{-2}$) relative to 2,000 dbar at 10 dbar in (a) July 2011 and (b) August 2011 from the grid point value of the monthly objective analysis using Argo data (Hosoda, Ohira, and Nakamura 2008). The S1 mooring site is at 30° N, 145° E and is indicated by the X. The rectangle outlined by the dashed line is examined in Figure 4. The color bar indicates the salinity scale.

into the thermocline as near-inertial internal waves (e.g., Gill 1984; Sanford, Price, and Girton 2011). It has been suggested that those internal waves propagate in the seasonal thermocline (e.g., Qiu et al. 2006) and create mixing at the base of the euphotic zone, which could enhance vertical fluxes of nutrients (e.g., Sukigara et al. 2011).

This is the second of a series of articles, of which Inoue et al. (2016) is the first (hereafter referred to as Part 1) and Kouketsu, Inoue, and Suga (2016) is the third (hereafter referred to as Part 3). Part 1 provides an overview of the S1-INBOX, during which a cyclonic eddy,

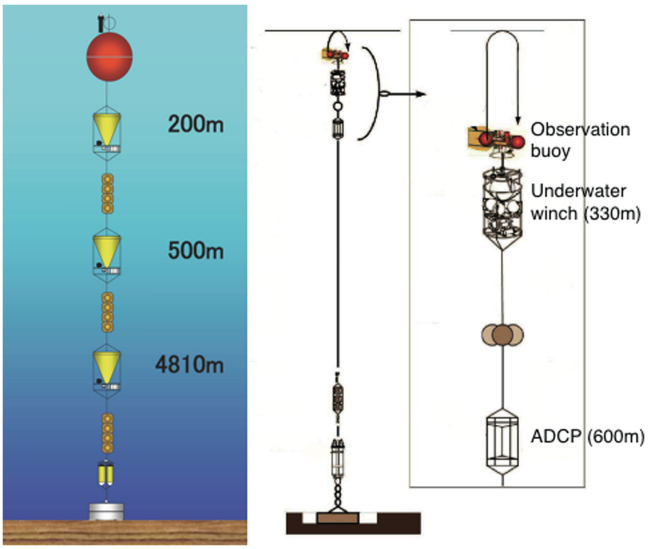

Figure 2. Design of the S1 mooring. The mooring on the left is for the sediment traps. The mooring on the right is for the underwater profiling buoy system. ADCP, acoustic Doppler current profiler.

typhoons, and an anticyclonic eddy influenced site S1. Our main goal here was to use the S1 biogeochemical moorings and shipboard measurements during the S1-INBOX study to describe the biogeochemical responses of the ocean to a weak cyclonic eddy and typhoons. The sampling methods used as a part of the S1 biogeochemical mooring study and the shipboard survey conducted by the R/V *Mirai* during the deployment of floats (MR11-05) are summarized in Section 2. In Section 3, results from the mooring are presented, and shipboard measurements conducted around the cyclonic eddy are used to support the mooring results. In Section 4, we discuss the effects of the cyclonic eddy and typhoons that passed by the S1 mooring site during the S1-INBOX study.

2. Data

a. S1 biogeochemical moorings

The S1 mooring site contained two moorings (Fig. 2): an underwater profiling buoy mooring (Fujiki et al. 2008, 2011) and a sediment trap mooring (Honda et al. 2013). The underwater profiling buoy mooring also included an acoustic Doppler current profiler (ADCP). The underwater profiling buoy system (Fujiki et al. 2008, 2011) was equipped with a submersible fast-repetition-rate fluorometer (FRRF; Diving Flash, Kimoto Electric, Osaka, Japan), a scalar irradiance sensor (QSP-2200, Biospherical Instruments, San Diego, CA), a conductivity-temperature-depth (CTD) sensor (MCTD, Falmouth Scientific, Cataumet, MA), and a DO sensor (Compact Optode, JFE Advantech, Nishinomiya, Japan). The sensor

DO values were adjusted to match the calibrated float DO profiles (see Appendix). To minimize instrument biofouling, an underwater winch was placed below the euphotic zone. The instruments moved between the winch depth and the surface at a rate of 0.2 m s^{-1} once every 3 days during the daytime (12:00 local time) and once every 6 days during the night (3:00 local time). The daytime samples were used in this study. The instrument package recorded vertical profiles of phytoplankton fluorescence, irradiance, temperature, salinity, and DO in the euphotic zone. The potential photochemical efficiency of photosystem II, the F_v/F_m ratio (Kolber, Praíšil, and Falkowski 1998), was measured with the FRRF and used as an index of photosynthetic activity. Here, F_v is the variable fluorescence, and F_m, the maximum fluorescence, is used to estimate the chlorophyll *a* concentration (Fujiki et al. 2008). We measured the F_v/F_m ratio from the dark chamber on the FRRF and focused on the F_v/F_m ratio near the base of the euphotic zone (~90 m), where the light level was low even in daytime, and nonphotochemical quenching should therefore have been minimal. Relatively high F_v/F_m ratios indicate that photosynthetic activity is enhanced, possibly because of an influx of nutrients (e.g., Bibby et al. 2008; Corno et al. 2008). The oxygen production rate, P_{O_2}, was estimated with the FRRF (Suggett, Maberly, and Geider 2006; also see equation 1 in Fujiki et al. 2008). The underwater profiling buoy mooring was also equipped with a CTD sensor. An upward-looking, 75 kHz ADCP (Workhorse Long Ranger, Teledyne RD Instruments, Poway, CA) was moored at a depth of approximately 600 m on the underwater profiling buoy mooring. The ADCP sampling interval was every 60 seconds, and the signal was averaged over every hour. The moored ADCP was able to measure current velocities with a vertical resolution of 8 m, but because of the side-lobe effect (e.g., Gordon 1996), only below a depth of 50 m. The ADCP data made it possible to identify candidate mechanisms for the transport of nutrients into the euphotic zone. Time-series sediment traps were set at 200 m (SMD26S-6000, NGK Ocean, Tokyo, Japan) and at 500 m and 4,810 m (Mark7G-21, McLane Research Laboratory Inc., East Falmouth, MA) on the S1 mooring. The sampling cup was automatically renewed every 16 days. Details of sampling and chemical analysis have been described in Honda et al. (2013, section 2) and at http://ebcrpa.jamstec.go.jp/k2s1/en/mst.html.

b. Overview of MR11-05 and sampling methods

The R/V *Mirai* arrived at and left the S1 mooring site on YDAY 203 (23 July 2011) and 211 (31 July 2011), respectively. The time interval is identified by the acronym YDAY, defined as time interval in days since 1 January 2011 (i.e., YDAY = 0 on 1 January 2011 [UTC]). Local time was UTC + 10 hours. A total of 12 floats were deployed during YDAYs 203–204. During YDAYs 204–209, nine CTD casts (casts 1–9) were completed, and the S1 biogeochemical moorings (sediment trap and underwater profiling buoy moorings) were replaced. During YDAYs 210–211, five CTD casts (casts 10–14) were conducted during six float deployments for calibration of the DO sensors. Floats were deployed around the S1 mooring to observe a cyclonic eddy during YDAYS 203–211 (see Part 1 for details of the float deployment).

Bottle samples were collected along with the CTD casts, and the water was used to measure nutrient concentrations, phytoplankton pigments, and primary productivity (PP). Concentrations of nitrate plus nitrite (hereafter nitrate) were measured with a continuous-flow analyzer (QuAAtro 2-HR, BL TEC K. K., Osaka, Japan). Chlorophyll *a* concentrations were measured with a fluorometer (model 10-AU, Turner Designs Inc., Sunnyvale, CA) by using the nonacidification fluorometric method of Welschmeyer (1994). For these assays, 0.5 L of water from each depth was filtered through a Whatman GF/F filter (Whatman International) under gentle vacuum (<0.020 MPa). The pigments on the filter were extracted with *N*, *N*-dimethylformamide at −20°C in the dark for 24 hours (Suzuki and Ishimaru 1990). We determined the abundance of different phytoplankton groups based on the concentrations of diagnostic pigments by using the CHEMTAX program (e.g., Mackey et al. 1996, 1997). For this analysis, phytoplankton pigments were analyzed with a high-performance liquid chromatography system (Agilent, Santa Clara, CA; Zapata, Rodríguez, and Garrido 2000). PP was estimated by using on-deck incubations, which were conducted for 24 hours starting at dawn in light-adjusted incubation bottles. Water samples were transferred to acid-cleaned polycarbonate bottles (1 L), and $NaH^{13}CO_3$ was added to each bottle before the incubation to achieve a final concentration of 0.2 mmol L^{-1}, which is sufficient to enrich the bicarbonate concentration to approximately 10%. After the incubation, water samples were filtered through precombusted GF/F filters, and inorganic carbon was removed by fuming with HCl. The ^{13}C content of the particulate fraction was measured with a mass spectrometer (ANCA-SL, SerCon Ltd., Cheshire, UK; Hama et al. 1983). The bottom of the euphotic zone was defined as the depth where the irradiance decreased to 1% of the surface irradiance (wavelengths of 400–700 nm). To determine this depth, we used data recorded by the sea-viewing wide field-of-view sensor (SeaWiFS) profiling multichannel radiometer and the SeaWiFS multichannel surface reference sensor (Satlantic LP, Halifax, Nova Scotia, Canada) during daylight hours on the day before seawater sampling.

A Knauer-type (Knauer, Martin, and Bruland 1979), cylindrical, drifting sediment trap array was deployed on YDAY 205 (20:10 UTC) and recovered on YDAY 210 (2:10 UTC). The traps were deployed at depths of approximately 60, 100, 150, and 200 m. The traps were assembled from eight transparent polycarbonate cylinders with a baffle to reduce turbulence at each depth. The collection area was 0.0038 m^2, and the aspect ratio (620 mm length/75 mm width) was 8.27. Details of the sampling and chemical analysis have been described in Honda et al. (2015) and http://ebcrpa.jamstec.go.jp/k2s1/en/dst.html.

Further details of the MR11-05 cruise and methods can be found in the cruise report (http://www.godac.jamstec.go.jp/darwin/cruise/mirai/MR11-05_leg1/e).

c. Environmental data

In this study, we used the 1/4° × 1/4° (latitude × longitude) daily gridded sea surface height anomalies (SSHAs) from the Archiving, Validation, and Interpretation of Satellite Oceanographic (AVISO) data set (Ducet, Le Traon, and Reverdin 2000). The altimeter

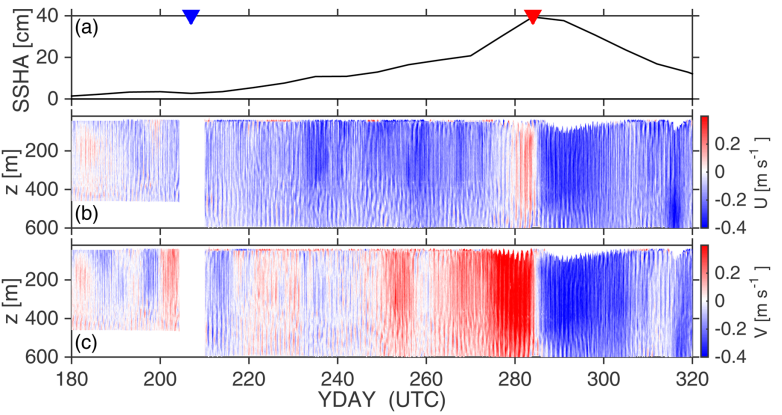

Figure 3. Time series of (a) weekly averaged sea surface height anomaly (SSHA) at the S1 mooring site, (b) zonal velocity U (m s^{-1}), and (c) meridional velocity V (m s^{-1}). Blue and red inverted triangles on the top indicate dates when the cyclonic and anticyclonic eddies approached the S1 mooring site, respectively. The horizontal axis is YDAY starting on 180 (30 June) and ending on 320 (17 November). The data gap between YDAYs 204 and 210 was because of the mooring replacement. YDAY, time interval in days since 1 January 2011.

products were produced by Ssalto/Duacs and distributed by AVISO, with support from the Centre National D'Etudes Spatiales Data Center (http://www.aviso.altimetry.fr/duacs/). We used 10 m wind speeds from the Japan Meteorological Agency (JMA) forecast model (Saito et al. 2006; Saito 2012). The temporal and spatial resolution of JMA winds obtained from the nonhydrostatic, mesoscale model were 1 hour, 0.0625° for zonal directions, and 0.05° for meridional directions, respectively. The large-scale properties shown in Figure 1 were obtained from the grid point value of the monthly objective analysis using Argo data, which gives temperature and salinity on a 1° × 1° horizontal grid by using a two-dimensional optimal interpolation on pressure surfaces (Hosoda, Ohira, and Nakamura 2008). The horizontal decorrelation radii of the optimal interpolation are set approximately 10° in midlatitudes near the sea surface, as indicated in Hosoda, Ohira, and Nakamura (2008, table 3).

3. Results

a. Biogeochemical responses to the cyclonic eddy observed at the S1 mooring

The features of a cyclonic eddy were apparent from examination of the ADCP data (Fig. 3) and a horizontal map of the SSHA (Fig. 4). A weak southwestward flow was observed before YDAY 220 (Fig. 3b and c); a relatively stronger westward flow was observed after YDAY 230 (Fig. 3b), when the northern edge of the cyclonic eddy passed the S1 mooring (Fig. 4a and b). At about YDAY 255 (Figs. 3b and 4c), a northward flow appeared when the eddy moved southwestward and left the S1 mooring site. There was a strong meridional flow at

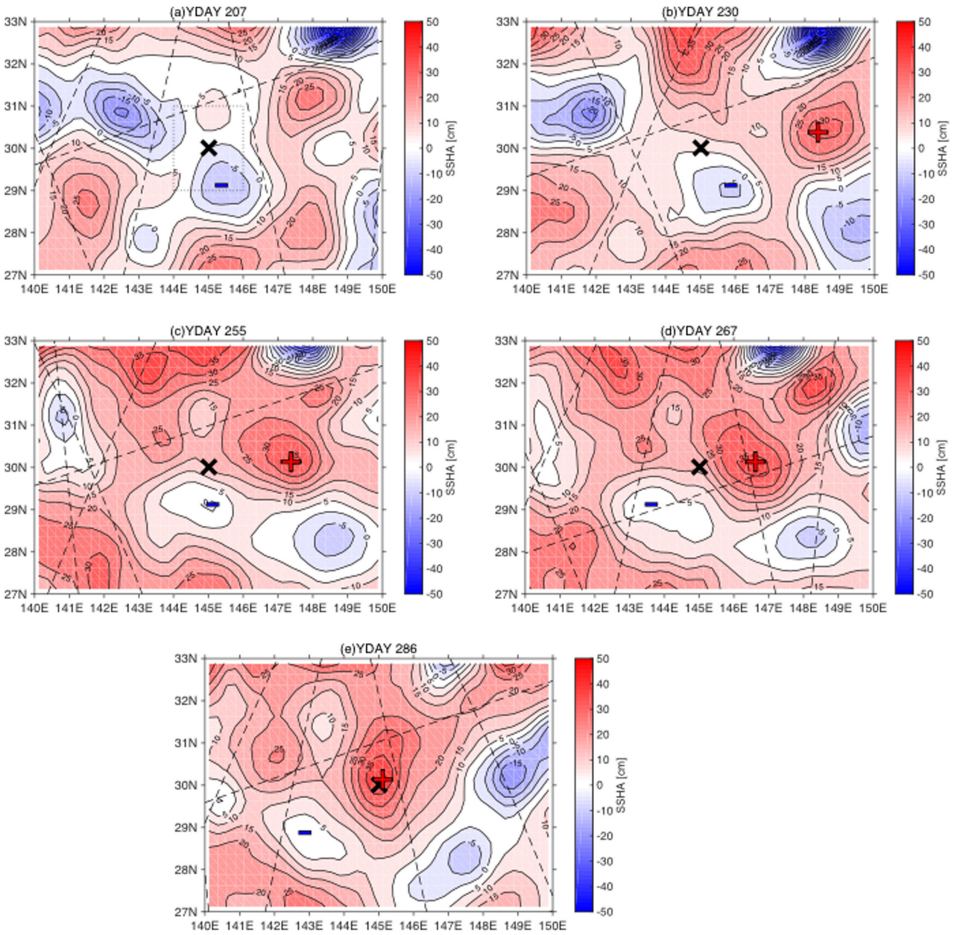

Figure 4. Sea surface height anomaly (SSHA) on (a) YDAY 207, (b) YDAY 230, (c) YDAY 255, (d) YDAY 267, and (e) YDAY 286. The color bar indicates the SSHA scale. Dashed lines indicate satellite paths. The S1 mooring site is shown by the X. The blue − and red + are centers of the cyclonic and anticyclonic eddies defined by the local SSHA minimum and maximum, respectively. The dotted rectangular box in (a) indicates the region shown in Figures 7 and 14. YDAY, time interval in days since 1 January 2011.

about YDAY 280 (Fig. 3c) associated with an anticyclonic eddy (Fig. 4d and e), which is described in the Appendix.

During the mooring observation, salinity values varied around 0.1 on the isopycnal surfaces on a time frame of about 1 week (Fig. 5a). The DCM was located at a depth of approximately 100 m (Fig. 5b). High chlorophyll *a* concentrations were observed (∼0.4, 0.7, and 0.4 mg m^{-3} on YDAYs 216, 234, and 267, respectively) when the depth of the

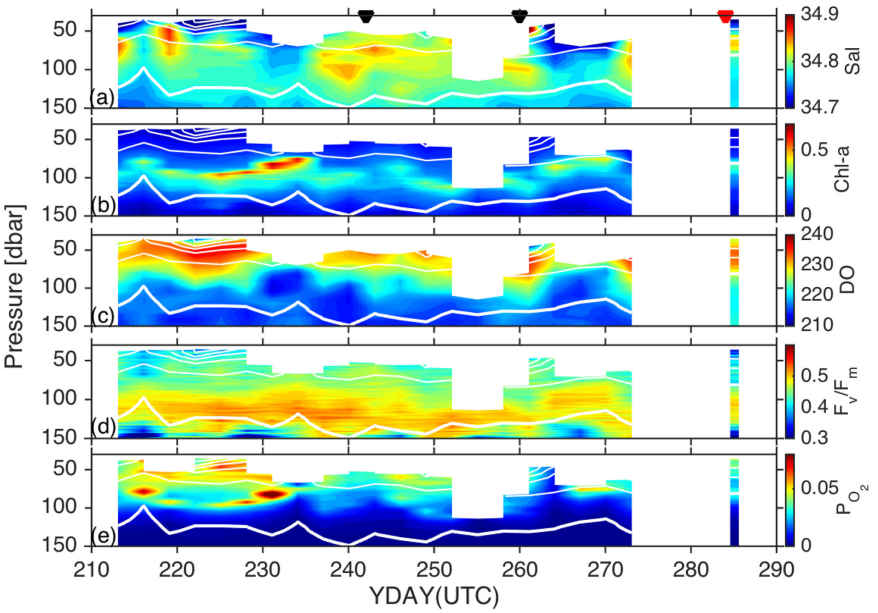

Figure 5. Time series (daytime sampling every 3 days) of (a) salinity (Sal); (b) chlorophyll *a* (Chl-*a*; mg m^{-3}); (c) dissolved oxygen (DO; μmol kg^{-1}); (d) potential photosynthetic activity, F_v/F_m; and (e) oxygen production rate, P_{O_2} (mmol O_2 m^{-3} h^{-1}) from the underwater profiling buoy system. White contours indicate σ_θ potential density ρ_θ-1000 kg m^{-3} with a contour interval of 0.5 kg m^{-3}. Thick white line indicates a σ_θ of 25.0 kg m^{-3}. The data gaps after YDAY 270 are because of the mooring tilt. The black and red inverted triangles on the top indicate the date when typhoons (TALAS and SONCA) and an anticyclonic eddy were closest to the S1 mooring site, respectively. YDAY, time interval in days since 1 January 2011.

DCM shoaled (a suggestion of better light conditions and possibly nutrient transport). Note that high chlorophyll *a* concentrations were often associated with low-salinity water. The SSHAs indicated that the uplifts of the sea surface on YDAYs 216 and 234 could be associated with the edge of the cyclonic eddy (Fig. 4b) and on YDAY 267 with the transition from the cyclonic eddy to the anticyclonic eddy (Fig. 4d). During both periods, the profiler did not reach the shallow oxygen maximum (SOM) layer, which was shallower than the DCM layer, as shown in Section 3b (Fig. 5c). High F_v/F_m ratios (≥0.5) below 100 m were recorded by the FRRF between YDAYs 220 and 240 and around YDAY 252 (Fig. 5d). The P_{O_2} was highest (>0.05 mmol O_2 m^{-3} h^{-1}) on YDAYs 216 and 231 (Fig. 5e).

The export fluxes at 200 m (Fig. 6c) were occasionally one order of magnitude larger than the fluxes at 500 and 4,810 m (Fig. 6d and e) and were highest (∼220 mg m^{-2} day^{-1}) between YDAYs 240 and 275. These high fluxes were comparable to the annual maximum fluxes observed in the winters of 2011 and 2012 at a depth of 200 m (M. Honda, personal communication). However, the flux of opal ($SiO_2 \cdot 0.4H_2O$), which is associated

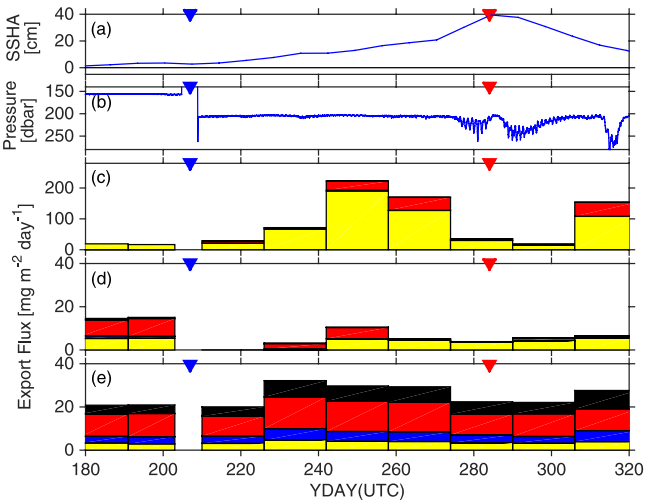

Figure 6. Time series of (a) weekly averaged sea surface height anomaly (SSHA); (b) depth of the shallowest sediment trap (target depth = 200 m; before the renewal of the mooring [YDAY 205], the pressure sensor was attached 50 m above the shallowest trap); and export flux at (c) 200 m, (d) 500 m, and (e) 4,810 m. Yellow is organic matter, blue is opal ($SiO_2 \cdot 0.4H_2O$), red is $CaCO_3$, and black is lithogenic matter. The blue (red) inverted triangles indicate the date when the cyclonic (anticyclonic) eddy was closest to the S1 mooring site. The data gap between YDAYs 203 and 210 is because of the mooring replacement. YDAY, time interval in days since 1 January 2011.

with diatom growth and which increased during the winter (M. Honda, unpublished data; http://ebcrpa.jamstec.go.jp/k2s1/en/), was low, and the flux was dominated by organic matter and $CaCO_3$ (Fig. 6c). A pressure sensor attached to the sediment trap at 200 m (Fig. 6b) showed that between YDAYs 240 and 275 the pressure was relatively stable, the suggestion being that the trap was not tilted down. Therefore, the collection efficiency may not have been compromised during the high flux between YDAYs 240 and 275.

b. Shipboard measurements of the cyclonic eddy during MR11-05

During the MR11-05 cruise (July 2011), six CTD casts (1–3, 7, 8, and 10) were conducted during 1 week (YDAYs 204–210) at the S1 mooring site (Figs. 4a and 7). CTD profiles 1, 2, and 3 revealed a different water mass (saline water) in the upper 100 m (Fig. 8). In profiles 7 and 8, low-salinity water was recorded in the upper 100 m. Bottle samples were also collected along with CTD casts 1, 2, 7, and 10 (Fig. 9). A DCM was apparent around a depth of 80 m, the SOM was shallower (30–80 m) than the DCM, and the nutricline was located at depths of 80–100 m. In profile 1, the high-nutrient, low-DO layer was observed at a depth of approximately 75 m.

PP and the phytoplankton community were assessed in profiles 2 and 7. Within the euphotic zone, profile 2 was relatively saline, and profile 7 was relatively fresh (Fig. 8). We

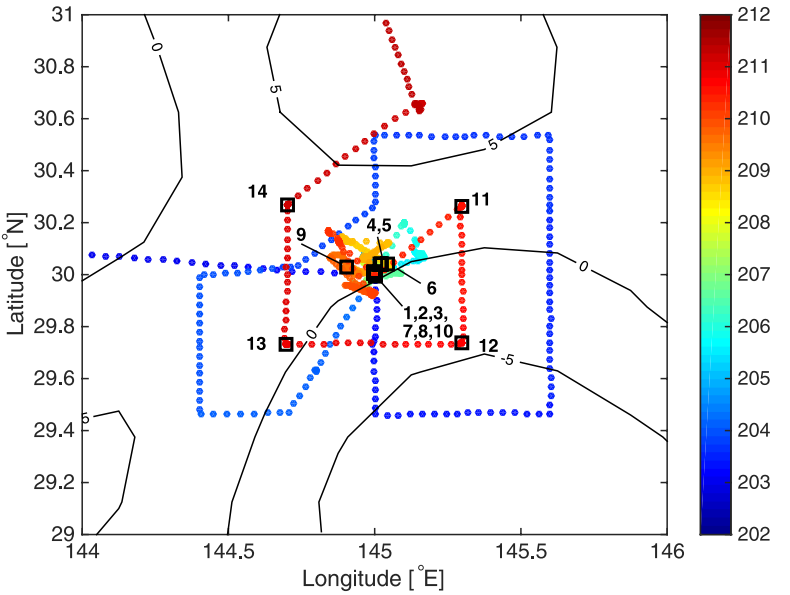

Figure 7. Map of ship tracks colored to indicate YDAY (color scale at right) and conductivity-temperature-depth (CTD) stations (black squares; bold numbers indicate CTD cast numbers). The sea surface height anomaly on YDAY 207 is superimposed (black contour lines). YDAY, time interval in days since 1 January 2011.

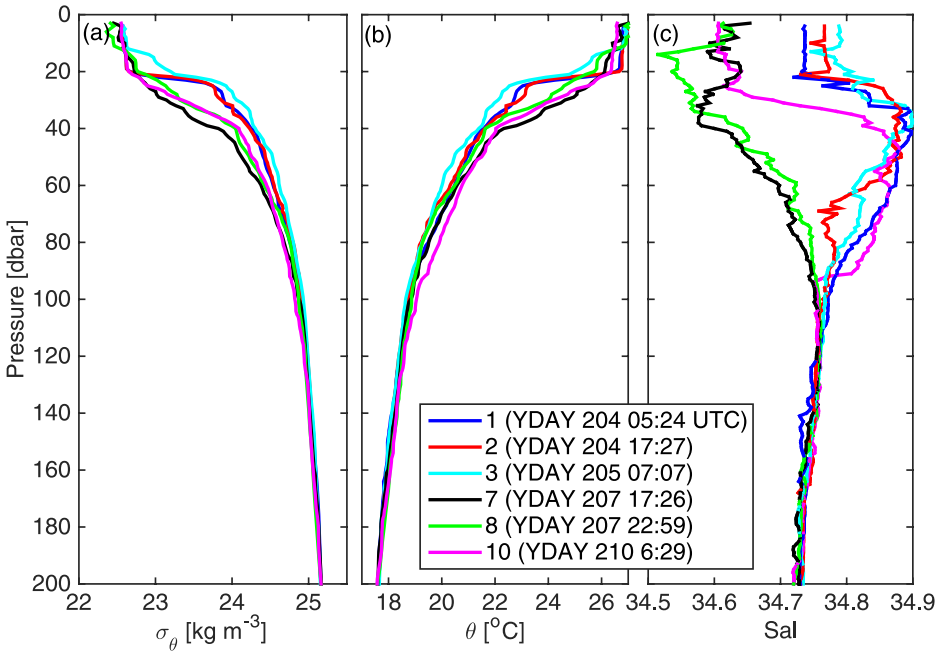

Figure 8. Vertical profiles of (a) sigma theta, σ_θ; (b) potential temperature, θ; and (c) salinity (Sal) from conductivity-temperature-depth casts at the S1 mooring. Profile numbers and YDAY (UTC) are color coded. Numbers after YDAY indicate hours and minutes. Local time is UTC + 10 hours. YDAY, time interval in days since 1 January 2011.

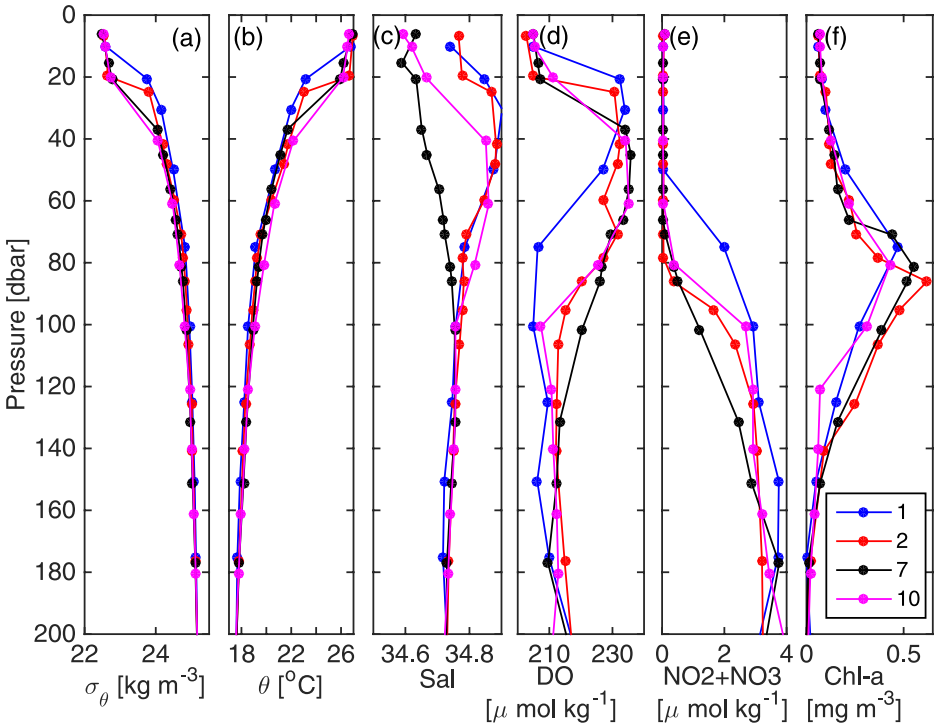

Figure 9. Vertical profiles of (a) Sigma theta, $\sigma_{\theta;}$ (b) potential temperature, θ; and (c) salinity (Sal) from conductivity-temperature-depth (CTD) casts. (d) Dissolved oxygen (DO), (e) nitrate (NO_2 + NO_3), and (f) chlorophyll *a* (Chl-*a*) from bottle samples. All of the samples were collected at the S1 mooring location. Colored dots indicate sample depths. CTD cast numbers are color coded.

found very little difference, however, in vertically integrated PPs (222 mg C m^{-2} day^{-1} for profile 2 and 227 mg C m^{-2} day^{-1} for profile 7) and chlorophyll *a* concentrations (16.5 mg m^{-2} for profile 2 and 19.1 mg m^{-2} for profile 7). The PP and chlorophyll *a* were integrated over the depth of the euphotic zone (95 m for profile 2 and 86 m for profile 7). Based on the CHEMTAX program, nano- and picophytoplankton, such as *Prochlorococcus* (29.6% and 30.2% of the chlorophyll *a* in profiles 2 and 7, respectively), prymnesiophytes (20.0% and 21.4%, respectively), and pelagophytes (19.4% and 22.6%, respectively), were the dominant classes of phytoplankton (Table 1), as was the case during the EDDIES study (e.g., Bibby et al. 2008). The species composition was similar in profiles 2 and 7 but there was a slight increase in size of 1–3 μm for profile 7 (Table 1). Calcareous microalgae known as coccolithophores are included among the prymnesiophytes, and their existence was confirmed by microscopy (not shown). Typhoon MA-ON passed by the S1 mooring site on YDAY 202 just before the cruise (fig. 14 in Part 1). It is unclear whether this typhoon

Table 1. The composition of the phytoplankton community and the distribution of phytoplankton cell sizes in profile 2 (YDAY 204) and profile 7 (YDAY 207) based on the chlorophyll standing stock. All percentages were estimated from samples vertically integrated over the depth of the euphotic zone. Chloro, chlorophytes; Crypto, cryptophytes; Cyano, cyanobacteria; Diato, diatoms; Dino, dinoflagellates; Pelago, pelagophytes; Prasino, prasinophytes; Prochloro, *Prochlorococcus*; Prymne, prymnesiophytes; YDAY, time interval in days since 1 January 2011.

	Size composition (%)				Group composition (%)								
Profile	>10 μm	3–10 μm	1–3 μm	<1 μm	Dino	Diato	Pelago	Prymne	Crypto	Prasino	Chloro	Cyano	Prochloro
2	10.3	11.3	28.8	49.6	2.5	2.4	19.4	20.0	2.7	6.7	6.3	10.4	29.6
7	11.8	10.6	34.6	42.9	2.0	1.9	22.6	21.4	1.6	4.0	4.5	11.9	30.2

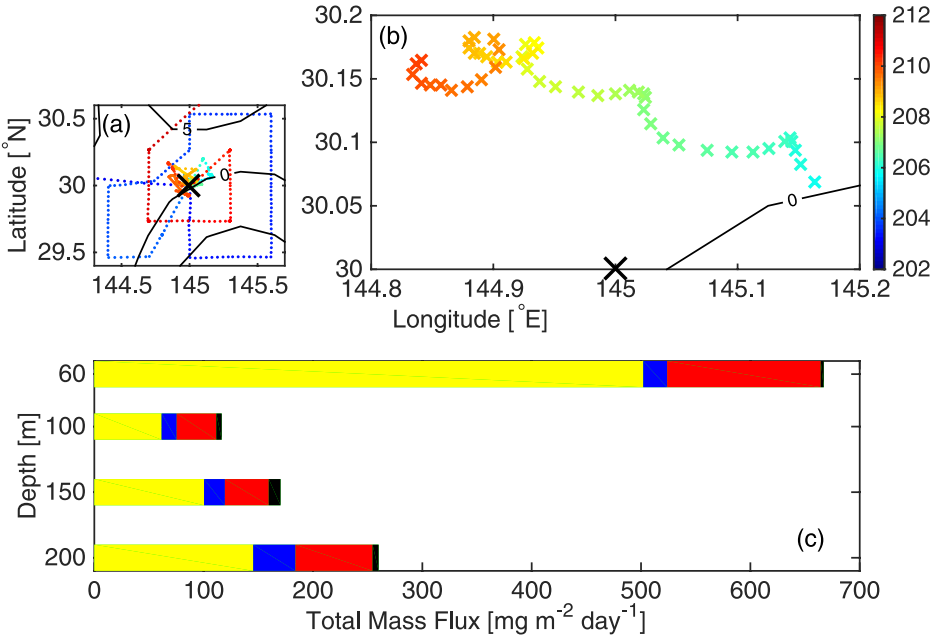

Figure 10. Map of (a) ship tracks shown in Figure 7 and (b) trajectory of the drifting sediment trap colored to indicate YDAY (color scale at right). The sea surface height anomaly on YDAY 207 is superimposed (black contours). The black X indicates the S1 mooring site. (c) Export flux into the drifting sediment traps. Yellow is organic matter, blue is opal ($SiO_2 \cdot 0.4H_2O$), red is $CaCO_3$, and black is lithogenic matter. YDAY, time interval in days since 1 January 2011.

enhanced PP during MR11-05. Determination of the dominant species after Typhoon MA-ON indicated that the typhoon did not lead to a diatom bloom.

A drifting sediment trap was launched northeast of the S1 mooring on YDAY 205 (20:10 UTC). The trap moved northwestward and was recovered on YDAY 210 (2:10 UTC) (Fig.

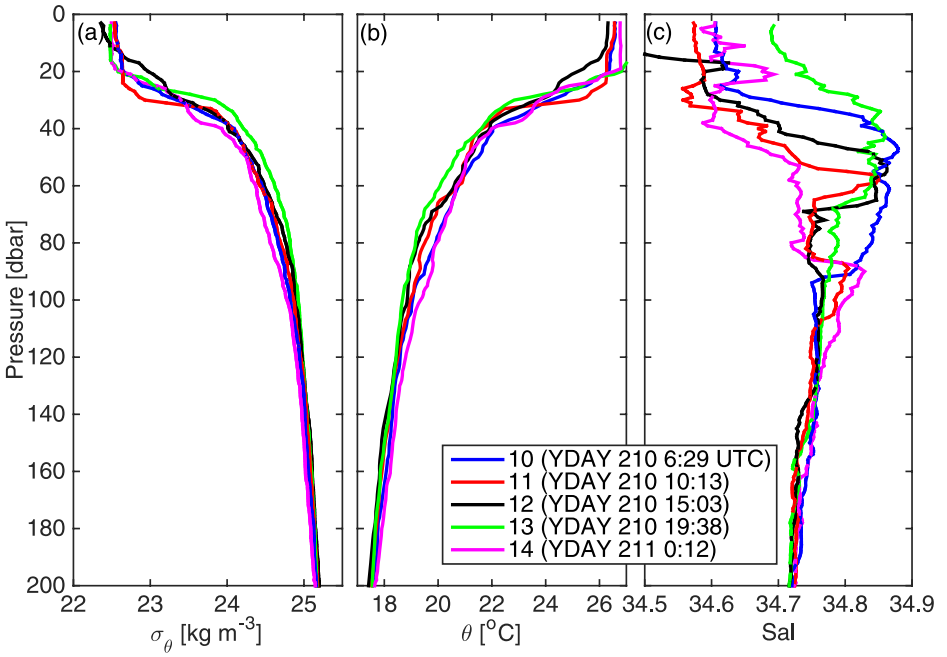

Figure 11. Vertical profiles of (a) sigma theta, σ_θ; (b) potential temperature, θ; and (c) salinity (Sal) during the deployment of S1-INBOX floats. Color coding indicates conductivity-temperature-depth cast numbers 10–14. Numbers after YDAY indicate hours and minutes. Local time is UTC + 10 hours. S1-INBOX, Western North Pacific Integrated Physical-Biogeochemical Ocean Observation Experiment conducted around the S1 biogeochemical mooring site; YDAY, time interval in days since 1 January 2011.

10). A comparison with the sediment trap moored at 200 m before YDAY 240 (Fig. 6c) showed that the composition of the material in both traps was similar: organic matter and $CaCO_3$ were dominant.

During YDAYs 210–211, CTD casts 10–14 were taken within a 1° × 1° area centered at the S1 mooring site (Fig. 7). These CTD profiles documented both temporal and spatial variability (Fig. 11). Profile 12 was conducted closest to the eddy center (southeast of site S1; Fig. 7). Above 50 m, high-salinity water was observed to the southwest of the S1 mooring in profile 13. Bottle samples showed water column characteristics similar to those at the S1 mooring site (Fig. 12): the nutricline was at depths of 80–100 m, as deep as or just below the DCM, and the SOM was at depths of 40–80 m. Note that at the site of CTD profile 10 (at the S1 mooring site), the nitrate concentration at 100 m was relatively high, and the DO concentration was relatively low. This pattern might have reflected vertical uplift because of the cyclonic eddy. In profile 11 (northeast of site S1), there was a water mass characterized by a low nitrate concentration at 100 m and by high concentrations of

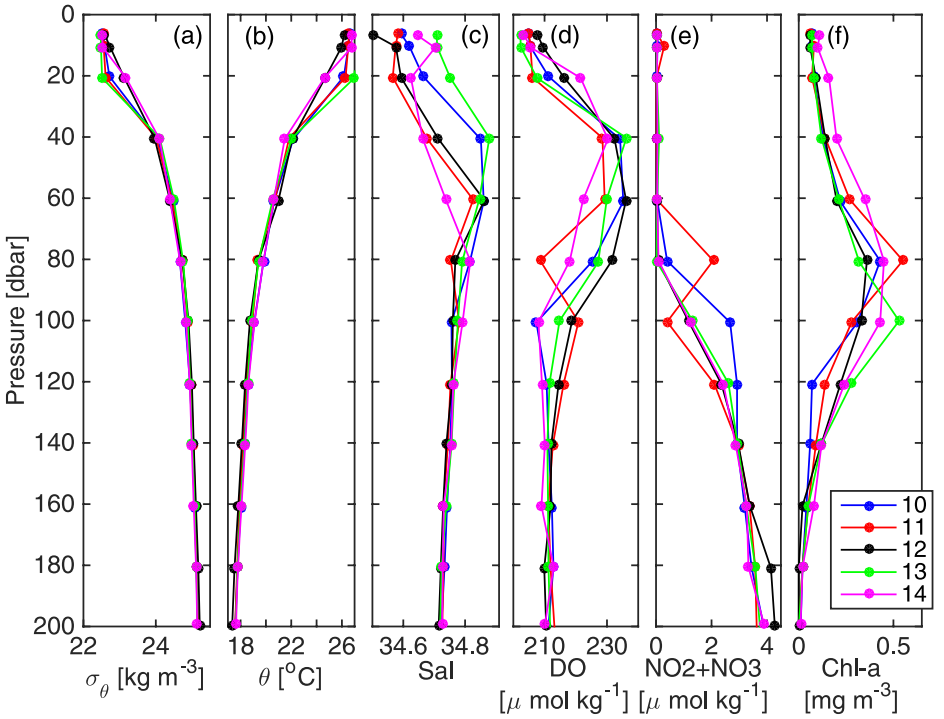

Figure 12. Vertical profiles of (a) sigma theta, σ_θ; (b) potential temperature, θ; and (c) salinity from conductivity-temperature-depth (CTD) casts. (d) Dissolved oxygen (DO), (e) nitrate ($NO_2 + NO_3$), and (f) chlorophyll *a* (Chl-*a*) from bottle samples. Color coding indicates CTD cast numbers 10–14.

nitrate and chlorophyll *a* and a low DO concentration at a depth of 80 m. This water mass corresponded to the intrusive structure of low-salinity water apparent in the CTD profile (Fig. 11). The oxygen and fluorometer data are not shown.

4. Discussion

a. Cyclonic eddies

The mooring and shipboard measurements recorded the same cyclonic eddy at slightly different times and locations. It is thus useful to compare results from the two sets of measurements and to identify the general features of the cyclonic eddy. Figure 13 shows that the water masses where we recorded shipboard CTD profile numbers 2 and 7 were the saltiest and freshest water masses, respectively. These profiles reflect conditions where we estimated PP and the composition of the phytoplankton community. Shipboard CTD profile 11 documented the intrusion of water with relatively low salinity and DO and relatively high chlorophyll *a* (Fig. 13d–f). The mooring CTD profiles documented water with intermediate values of salinity, DO, and chlorophyll *a* (Fig. 13a–c). The profile on YDAY 228

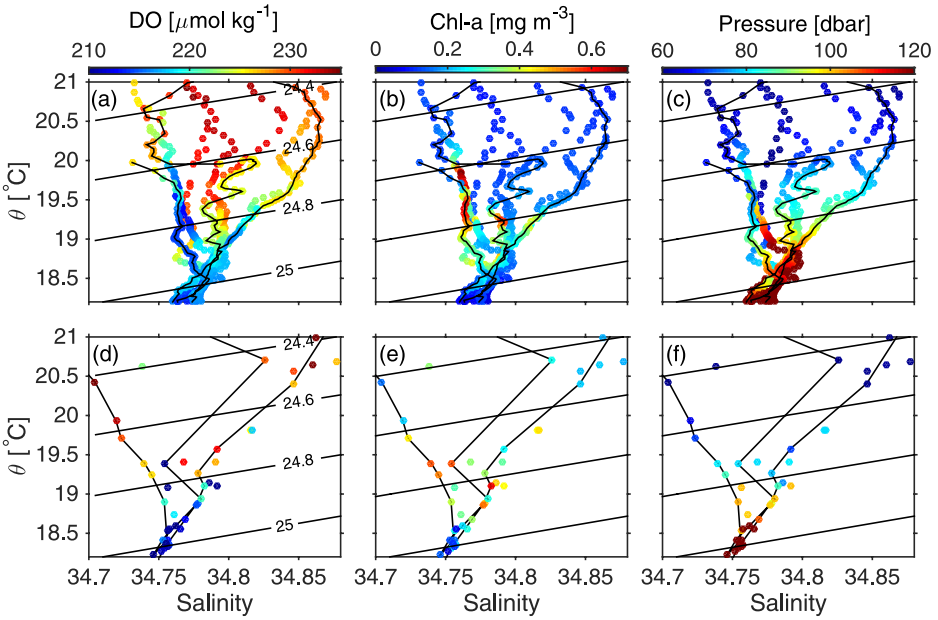

Figure 13. Potential temperature (θ)–salinity (*S*) diagrams from (a–c) the moored conductivity-temperature-depth (CTD) on the S1 mooring and (d–f) bottle samples taken during the shipboard CTD profiles. Colors in (a) and (d) indicate dissolved oxygen (DO); in (b) and (e), chlorophyll *a* (Chl-*a*); and in (c) and (f), pressure. Color bars on the top show values of those variables. The thin lines in (a–c) are the profiles taken on YDAY 234 (left), YDAY 228 (middle), and YDAY 213 (right), respectively. Those in (d–f) are profile 7 (left), profile 11 (middle), and profile 2 (right), respectively. YDAY, time interval in days since 1 January 2011.

recorded relatively high salinity, DO, chlorophyll *a*, and pressure within intrusive structures. The profile on YDAY 234 recorded relatively fresh water with lower DO and higher chlorophyll *a* concentrations. There might be a tendency for low-salinity water to have higher chlorophyll *a* concentrations (YDAYs 213 and 234 in Fig. 13b). However, lower pressures on the same isopycnal surfaces on YDAYs 213 and 234 of the time series (Fig. 5) imply uplift of deeper water. The implication is that the ship and mooring data sets recorded highly variable structures around the edges of the cyclonic eddy. Water mass variability was also apparent in the sea surface temperature and salinity observed during the cruise (Fig. 14). Salinity changes of more than 0.1 were observed over a period of 1 week, for example, at 29.7° N, 145° E. A salinity change of similar magnitude was also observed over a spatial scale of 20–50 km within the same day. The large-scale salinity change apparent in Figure 1 indicates that the low-salinity water may have been advected from the north.

It is also important to note the cause of the increased export flux during the period when the chlorophyll *a* concentration in the DCM was relatively high (YDAY 220–270 in Fig. 5).

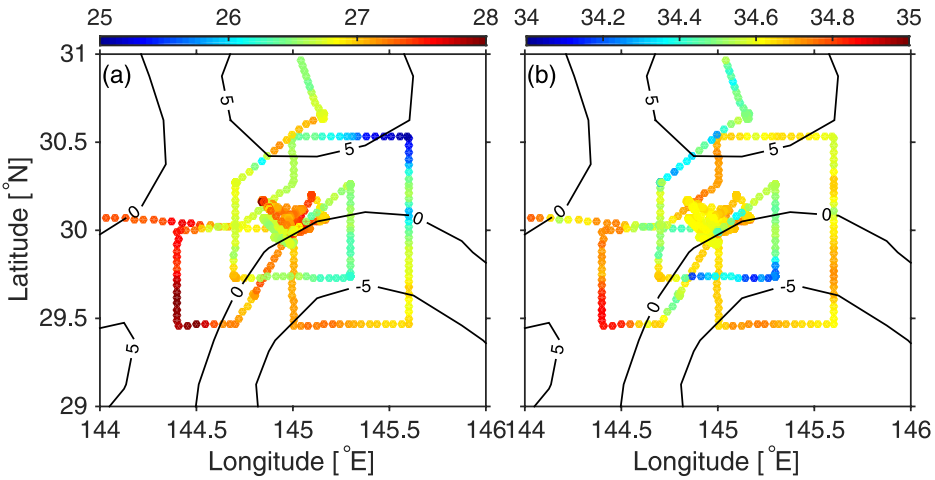

Figure 14. Map of (a) ship tracks colored to indicate sea surface temperature and (b) sea surface salinity. Color bars on the top of each figure show values. The sea surface height anomaly on YDAY 207 is superimposed (black contours). YDAY, time interval in days since 1 January 2011.

A sediment trap sample recorded the flux for a period of a few weeks, and the profiler recorded conditions instantaneously every 3 days. Based on the transit time of radiocesium from the surface to a depth of 500 m, which was derived from studies after the Fukushima Daiichi Nuclear Power Plant accident, Honda et al. (2013) pointed out that the speed of sinking particles between the surface and a depth of 500 m was possibly 26–71 m day^{-1} at the S1 mooring site. It would therefore have taken 2–5 days for particles to sink from the DCM (at depths of 80–100 m in Fig. 5b) to a depth of 200 m. The on-deck incubation experiment at the S1 mooring site during MR11-05 indicated that the phytoplankton production started to increase 2–4 days after water sampling at the DCM (T. Fujiki, unpublished data). A time interval of 2–4 days is within the duration of the period when the highest flux was observed. The highest flux could therefore be associated with the cyclonic eddy. Because the core of the cyclonic eddy did not pass by the S1 mooring, this large export flux could be related to nutrient transport by a combination of vertical movement at the edge of the eddy and horizontal advection. Because a steady westward flow ($\sim$0.3 m s^{-1}) at the northern edge of the cyclonic eddy was observed during this period (Figs. 3b and 4a and b), we hypothesize that particles were advected from upstream by a distance equal to one-fourth of the circumference of the eddy with a time frame of 1 week.

Although there were two types of water masses during the S1-INBOX experiment, phytoplankton composition was similar in the two water masses. Those water masses did not lead to a diatom bloom. Such a bloom occurred in an anticyclonic, mode-water eddy during the EDDIES experiment, when the wind-current interaction persistently transported nutrients into the euphotic zone at the eddy center (e.g., McGillicuddy et al. 2007). Rather,

during S1-INBOX, the phytoplankton composition was similar to that observed around the edge of eddies during the EDDIES experiment (Bibby et al. 2008). It seems likely that *Prochlorococcus*, which is the smallest phytoplankton, could have become dominant during the MR11-05 cruise by using the limited supply of regenerated nitrogen when conditions were oligotrophic in the summer. However, it is possible that prymnesiophytes and pelagophytes, which are smaller than diatoms, could become dominant if nitrate is supplied intermittently because small phytoplankton have an advantage in terms of resource acquisition when nutrient concentrations are low (Raven 1998; Marañón 2015). *Prochlorococcus* generally cannot use NO_3 and requires regenerated nitrogen such as NH_4, although some exceptions can be found in Martiny, Kathuria, and Berube (2009). Other phytoplankton can use a variety of nitrogen sources. The implication is that intermittent nutrient transport, suggested by the relatively high F_v/F_m ratios (e.g., Bibby et al. 2008; Corno et al. 2008), enhanced the growth of phytoplankton such as prymnesiophytes, some of which have a calcium carbonate shell (Table 1), and the possible result was an increase of the export flux to 200 m because of the ballasting effect of the $CaCO_3$. This supposition is supported by the dominant components of the export flux into two independent sediment traps (Figs. 6 and 10).

We note that there was a difference between the export flux into the moored sediment trap and the flux into the drifting sediment trap. This inconsistency could be attributable to differences in the collection efficiencies of the different sediment traps and to contamination by swimmers (Honda et al. 2015). It is also possible that the drifting sediment trap captured some intermittent, high-production events because it sampled on a Lagrangian rather than Eulerian basis.

b. Typhoons

Three typhoons (MA-ON, TALAS, and SONCA) passed near the S1 mooring just before and during the S1-INBOX study on YDAYs 202, 241, and 260 (Fig. 15a), respectively, when the cyclonic eddy was near the S1 mooring site (e.g., Figs. 3a and 4). It is possible that those typhoons were associated with the high DCM values on YDAYs 216–234 and 267 (Fig. 5b). Here, we consider two processes that could have brought nutrients into the euphotic zone: (1) Ekman pumping and the horizontal kinetic energy associated with near-inertial oscillations in the mixed layer during the forced stage and (2) the propagation of near-inertial waves into the seasonal thermocline and subsequent mixing just below the euphotic zone during and after the relaxation stage in YDAYs 195–270.

The Ekman vertical velocity can be expressed as follows:

$$w_{Ek} = \frac{1}{\rho f}\left(\frac{\partial \tau_y}{\partial x} - \frac{\partial \tau_x}{\partial y}\right). \tag{1}$$

The parameter ρ is the surface density, and we assigned it a typical observed value of 1,022.5 kg m^{-3} (e.g., Fig. 8) for simplicity. The parameter f_0 is the Coriolis frequency at 30° N.

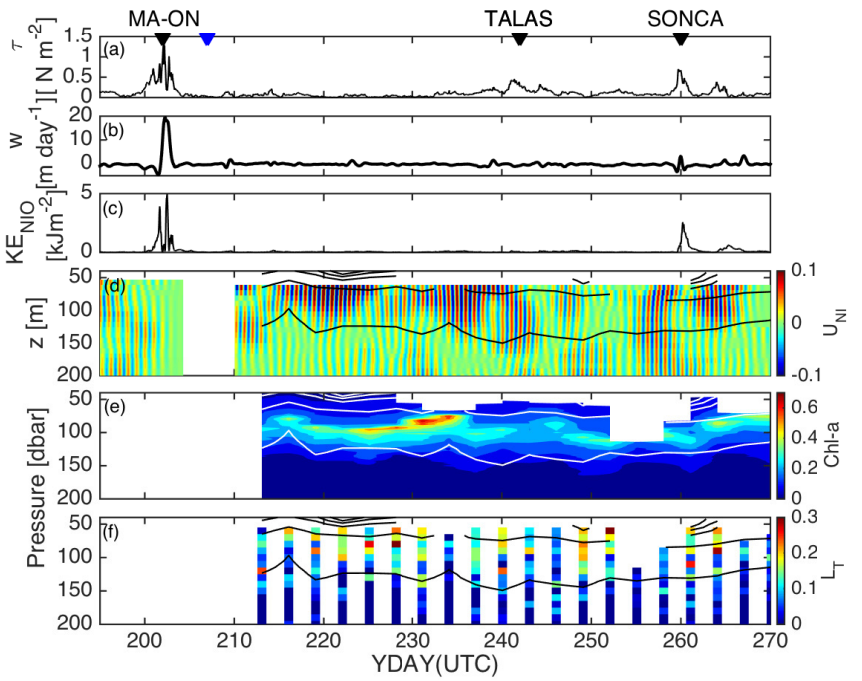

Figure 15. Time series of (a) the magnitude of the JMA wind stress, τ; (b) vertical velocity because of Ekman pumping from equation (1); (c) horizontal kinetic energy of inertial oscillations from equation (2); (d) band-passed (0.9–1.2 cycles per day) zonal velocity from the moored ADCP (m s^{-1}); (e) chlorophyll *a* (Chl-*a*; mg m^{-3}); and (f) Thorpe scales (dbar) averaged over 10 dbar and plotted every 10 dbar for presentation purposes. Contours in (d), (e), and (f) are σ_θ with a contour interval of 0.5 kg m^{-3}. The lowest line shows σ_θ= 25.0 kg m^{-3}. Pressure was used for the vertical axis of potential density. The data gap between YDAYs 203 and 210 in (c) is the period when the mooring was replaced. The black and blue inverted triangles on the top indicate the date when typhoons (MA-ON, TALAS, and SONCA) and the cyclonic eddy were closest to the S1 mooring site, respectively. ADCP, acoustic Doppler current profiler; JMA, Japan Meteorological Agency; YDAY, time interval in days since 1 January 2011.

The parameters τ_x and τ_y are the zonal and meridional components of the wind stress, respectively, calculated from 1-day, low-pass-filtered JMA winds and the parameterization by Large and Pond (1981) without considering an effect of surface currents. Eddy-Ekman pumping was ignored in this analysis because in a cyclonic eddy this pumping suppresses the upward delivery of nutrients, which was our main focus (e.g., McGillicuddy et al. 2007).

The maximum upward velocities of w_{Ek} (~20 m day^{-1}) were created by Typhoon MA-ON (Fig. 15b). The vertical migration of profiles seen in CTD casts 1–3 (Fig. 8) could therefore be because of Ekman upwelling and near-inertial pumping. However, the fact that this uplift was not observed after the casts suggests that the effect of the vertical uplift

caused by Typhoon MA-ON was brief. The other two typhoons caused only small upward velocities, occasionally O (1 m day^{-1}) for w_{Ek}. For the slow-moving Typhoon TALAS, the Ekman velocity was small at the S1 mooring site. It is therefore likely that the southward movement of the cyclonic eddy caused changes in the DCM (Fig. 15e) after passage of Typhoon TALAS on YDAY 240, at which time the doming isopycnal surface around 80 m and the DCM vanished.

We estimated the energy available to generate near-inertial internal waves by using wind data and a slab mixed-layer model (e.g., Pollard and Millard 1970; D'Asaro 1985). Following the formulation of D'Asaro (1985), we wrote the momentum equation in complex notation $Z = u + iv$, $T = (\tau_x + i\tau_y)/\rho$, and $\omega = r + if$,

$$\frac{dZ_I}{dt} + \omega Z_I = -\frac{dZ_E}{dt} = -\frac{1}{\omega}\frac{d}{dt}\left(\frac{T}{H}\right). \tag{2}$$

Here, Z_I is the damped inertial oscillations, Z_E is the Ekman current, and $Z = Z_I + Z_E$. Parameter T is the wind stress acting on the mixed layer; parameter H is the mixed-layer depth approximated by a second-order polynomial fit to the average mixed-layer depth obtained from the S1-INBOX floats as a function of time; and r is a decay rate, which we assumed to be $1/r = 3$ days. The relative vorticity (Weller 1982) was ignored for simplicity. Equation (2) was integrated from YDAY 181, and the inferred horizontal kinetic energy, $KE = (\rho H/2)|Z_I|^2$, was used to determine when inertial motions could be generated (Fig. 15c). Typhoons MA-ON (YDAYs 200–205) and SONCA (YDAY 260) could have generated strong inertial oscillations. After those surface oscillations, the band-passed ADCP velocities indicated that there were near-inertial currents above 150 m after YDAYs 210 and 260 (Fig. 15d). Those currents gradually dissipated or propagated into the thermocline. It is also possible that those waves were propagated horizontally and arrived at the S1 mooring site.

To clarify the roles of near-inertial waves and subsequent mixing on nutrient transport, we calculated the Thorpe scale (Thorpe 1977), L_T, from CTD upcast data as an indicator of mixing (see Appendix). The high DCM patches recorded by the underwater profiling buoy system (Fig. 15e) also corresponded to the near-inertial waves (Fig. 15d) and relatively large overturns (YDAYs 220–230 and 260–270) in Figure 15f, the indication being that, in addition to the cyclonic eddy, near-inertial waves and subsequent mixing generated by Typhoons MA-ON and SONCA might have played a role in the intermittent supply of nutrients. Around those mixing patches, averaged L_T scales varied from 0.1 m to 0.4 m. The square of the buoyancy frequency, N^2, calculated from reordered density, varied from 2×10^{-5} to 1×10^{-4} s^{-2} and was smaller below a depth of 120 m. The vertical diffusivity, K_ρ, at the base of the euphotic zone was very roughly estimated from the turbulent kinetic energy dissipation rate, $\varepsilon = 0.64 L_T^2 N^3$, and $K_\rho = \varepsilon\Gamma N^{-2} = 0.64\Gamma L_T^2 N$ by assuming mixing efficiency of $\Gamma = 0.2$ (e.g., Dillon 1982). It was estimated to be $0.64 \times 0.2 \times (0.2 \times 0.2) \times 10^{-2} \sim 5 \times 10^{-5}$ m^2 s^{-1} in those patches with L_T and N values of 0.2 m and 10^{-2} s^{-1}, respectively. Although this estimate is very rough, it could be used

to provide an average diffusivity and to quantitatively infer effects of diapycnal mixing on biogeochemical phenomena such as the temporally averaged new production recorded by the moored sediment trap.

If we assume that nutrient was transported into the euphotic zone by vertical mixing, there was no nutrient flux at the sea surface, all nutrient flux at the base of the euphotic zone was immediately used for new production, and the export flux at 200 m equaled the vertically integrated changes in the biomass in the euphotic zone, then the nutrient budget in the euphotic zone can be written as

$$C_{ex} = \frac{\partial}{\partial t}\int C\, dz = \int \gamma_{\mathrm{C:N}} \frac{\partial}{\partial z}\left(K_v \frac{\partial Ni}{\partial z}\right) dz = \gamma_{\mathrm{C:N}} K_v \frac{\partial Ni}{\partial z}, \tag{3}$$

where C_{ex} is the export flux of organic carbon from the moored sediment trap between YDAYs 242 and 258 (Fig. 6c), $\sim 62.5/86{,}400 = 7.2 \times 10^{-4}$ mg m^{-2} s^{-1}; $\gamma_{\mathrm{C:N}}$ is the molar Redfield ratio between carbon and nitrate, 106:16 (Redfield, Ketchum, and Richards 1963); K_v is the average vertical diffusivity of 5×10^{-5} m^2 s^{-1} estimated above; and $\frac{\partial Ni}{\partial z}$ is the vertical gradient of nitrate concentration approximately estimated from the bottle samples shown in Figs. 9 and 12, $\sim$2.5 μmol kg^{-1}/60 m = 0.042 μmol kg^{-1} m^{-1}. Dimensional adjustments were then made by using a seawater density of 1,025 kg m^{-3} and a molar mass of 12×10^3 mg mol^{-1} for carbon. With these adjustments, the right-hand side of equation (3) becomes $\gamma_{\mathrm{C:N}} K_v \frac{\partial Ni}{\partial z} = (106/16) \times (5 \times 10^{-5}) \times (0.042 \times 10^{-6}) \times (1{,}025 \times 12 \times 10^3) \approx 1.7 \times 10^{-4}$ mg C m^{-2} s^{-1} $\approx$ 14.8 mg C m^{-2} day^{-1}. This result suggests that diapycnal mixing could have accounted for roughly about one-fifth of the export flux between YDAYs 242 and 258.

In the absence of a change in the vertically integrated biomass within the euphotic zone from YDAYs 242 to 258, the export flux at 200 m would equal new production over that time interval, and the average diffusivity could have accounted for about one-fifth of that export flux. However, it was unclear if diapycnal mixing or vertical heaving because of the cyclonic eddy caused shorter-term temporal variability of the DCM layer (Fig. 15e). On the one hand, there appeared to be a tendency for the chlorophyll *a* concentrations to be higher when the depths of isopycnal surfaces were shallower (Fig. 16a–d). On the other hand, relatively high vertical diffusivities were intermittent (Fig. 16c and e). It is possible that the relatively short-term temporal variability of the high-chlorophyll DCM layer was associated with uplifting of isopycnal surfaces. Diapycnal mixing could further modify the DCM layer. Because this speculation is based on one event, observation of many events and application of tests for statistical significance would be necessary to test this hypothesis.

5. Summary

In this article, we reported results from the S1 moorings during S1-INBOX and from the shipboard biogeochemical surveys conducted by the R/V *Mirai* during the deployment of floats. The focus of this article was on the effects of a weak cyclonic eddy that was influenced by the passage of three typhoons. Results can be summarized as follows.

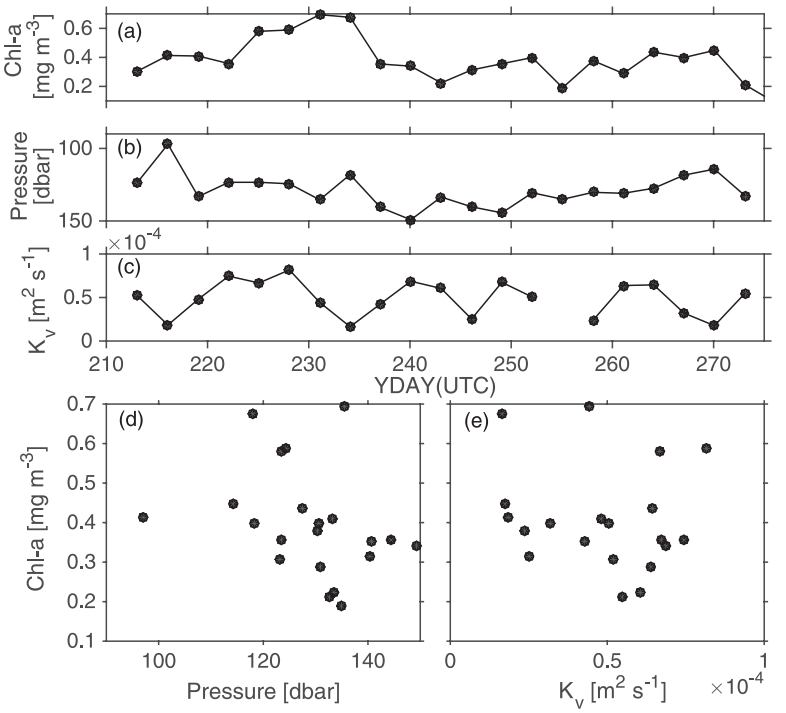

Figure 16. Time series of the (a) maximum chlorophyll *a* (Chl-*a*) concentration at the deep chlorophyll maximum layer, (b) pressure on the isopycnal surface $\sigma_\theta = 25$ kg m^{-3}, and (c) diapycnal diffusivities averaged over 80–100 dbar. The scatter plots of (d) the maximum chlorophyll *a* concentration and the pressure on the isopycnal surface, and (e) the maximum chlorophyll *a* concentration and the average diapycnal diffusivities.

The underwater profiling buoy system and ADCP suggested that high chlorophyll *a* concentrations occurred when the DCM was uplifted at the edge of the cyclonic eddy. High DCM values and F_v/F_m ratios were consistent with the supposition that upward or horizontal transport of nutrients was related to the highest export fluxes observed in the moored sediment trap. Shipboard measurements were conducted around the cyclonic eddy. Bottle samples showed that a DCM was present at approximately 80 m, the SOM (30–80 m) was shallower than the DCM, and the nutricline was located between 80 and 100 m. The fact that the dominant groups of phytoplankton were *Prochlorococcus*, prymnesiophytes, and pelagophytes suggests that during oligotrophic conditions in the summer, prymnesiophytes and pelagophytes can respond to intermittent nutrient supplies, a conclusion consistent with results of the EDDIES study (Bibby et al. 2008). The components of the export fluxes were similar in both the drifting and moored traps: organic matter and $CaCO_3$ were dominant, a result consistent with phytoplankton surveys during MR11-05.

Surface wind forcing could have generated near-inertial oscillations in the mixed layer during passages of Typhoons MA-ON and SONCA. Band-passed velocities indicated that near-inertial internal waves propagated vertically and horizontally into the seasonal thermocline. These internal waves and observed overturns were also related to high-chlorophyll DCM patches as well as to high export fluxes around the cyclonic eddy. A comparison between the export flux and nitrate flux during this period indicated that diapycnal mixing could have accounted for about one-fifth of the new production.

Although the mooring and shipboard measurements captured physical and biogeochemical processes around the edge of the cyclonic eddy, the spatial and temporal scales of these processes were approximately less than 50 km and 1 week, respectively. It was therefore difficult to distinguish three-dimensional processes with the discrete shipboard samplings and single-point mooring survey. This issue and nutrient transport by the eddy are further addressed in Part 3.

Acknowledgments. We are indebted to the captain, crew, and other scientists on the R/V *Mirai* cruises for their invaluable help in collecting data. Comments from reviewers greatly improved the manuscript. S. Kouketsu was partly supported by JSPS KAKENHI grant no. 12024485.

APPENDIX

a. Oxygen correction for the underwater profiling buoy system

Without sufficient calibration, the oxygen concentrations determined by the underwater profiling buoy system (O_{UPBS}; thin curves in Fig. A1) were different from the concentrations determined with the floats (O_{FLT}; thick curves in Fig. A1). The latter were calibrated with in situ shipboard conductivity-temperature-depth-dissolved oxygen (CTDO) observations conducted during the floats deployment (Part 1). Assuming that the differences depended on the oxygen absolute values and offsets, we obtained the corrected oxygen concentrations determined by the underwater profiling buoy system by fitting a straight line ($O_{CORR} \sim O_{FLT} = aO_{UPBS} + b$) to the float profiles close to the mooring. These float profiles were profiles determined within 2 days and 0.05° of latitude and longitude from the profiles obtained with the underwater profiling buoy system. The corrected profiles ($a = 0.54$ and $b = 91$) were similar to the float profiles, and the shallow oxygen maximum (SOM) values were reasonable (Fig. A1). However, the temporal drifts of the oxygen sensor on the underwater profiling buoy system and the quality of the corrected data could not be sufficiently evaluated because there were only two float profiles near the mooring in this study.

b. Anticyclonic eddy

Strong flows tilted down the sediment trap and underwater profiling buoy moorings (e.g., YDAY [time interval in days since 1 January 2011] 255 in Fig. 5 and YDAYs 275–300 in Figs. 5 and 6). Therefore, only one profile was recorded near the center of the anticyclonic eddy (YDAY 285 in Fig. A2). The σ_θ data indicated that isopycnal surfaces in the

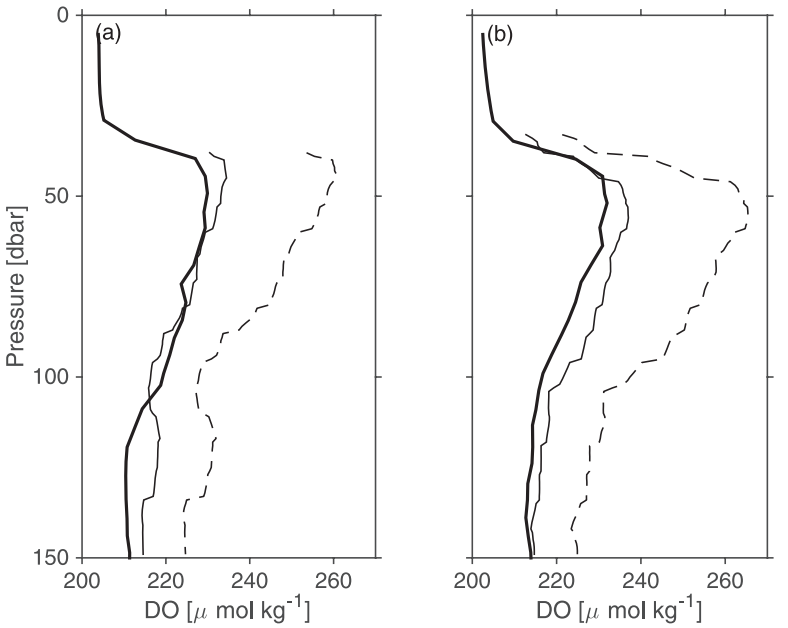

Figure A1. Oxygen profiles measured by the underwater profiling buoy system. Dashed and solid lines are before and after the calibration correction, respectively. To obtain the fitting coefficients, we used two pairs of oxygen profiles for comparison. (a) One was taken on YDAY 220 by float SN170, which was compared with that taken on YDAY 219 by the underwater profiling buoy system. (b) The other pair was taken on YDAY 222 by SN197 and the underwater profiling buoy system. The oxygen profile measured by the float is shown by the thick solid line. DO, dissolved oxygen; YDAY, time interval in days since 1 January 2011.

observed depth range were shallower than in the surrounding water. The dissolved oxygen concentration below the SOM was also higher near the eddy center than in the surrounding water. This information together with the low stratification below 100 m suggests that this anticyclonic eddy could have been a mode water eddy. The deep chlorophyll maximum layer was above 100 m, but it was slightly lower than during other periods. The fact that during the passage of the anticyclonic eddy the export flux into the moored sediment trap at 200 m was lower than during other periods (Fig. 6) possibly suggests a reduction of primary production (PP) because of lower transport of nutrients into the euphotic zone. However, it is also possible that the trapping efficiency was low in the anticyclonic eddy because of tilting of the sediment trap or that calcifying prymnesiophytes, which have a high sinking rate, were not stimulated by the anticyclonic eddy. We have only one profile because of the tilt caused by the strong flows, which also affected the collection efficiency of the sediment trap, and we have no shipboard measurements during the passage of the anticyclonic eddy. It was therefore impossible for us to identify the causes of the lower export flux. Further study is needed to understand PP in anticyclonic eddies.

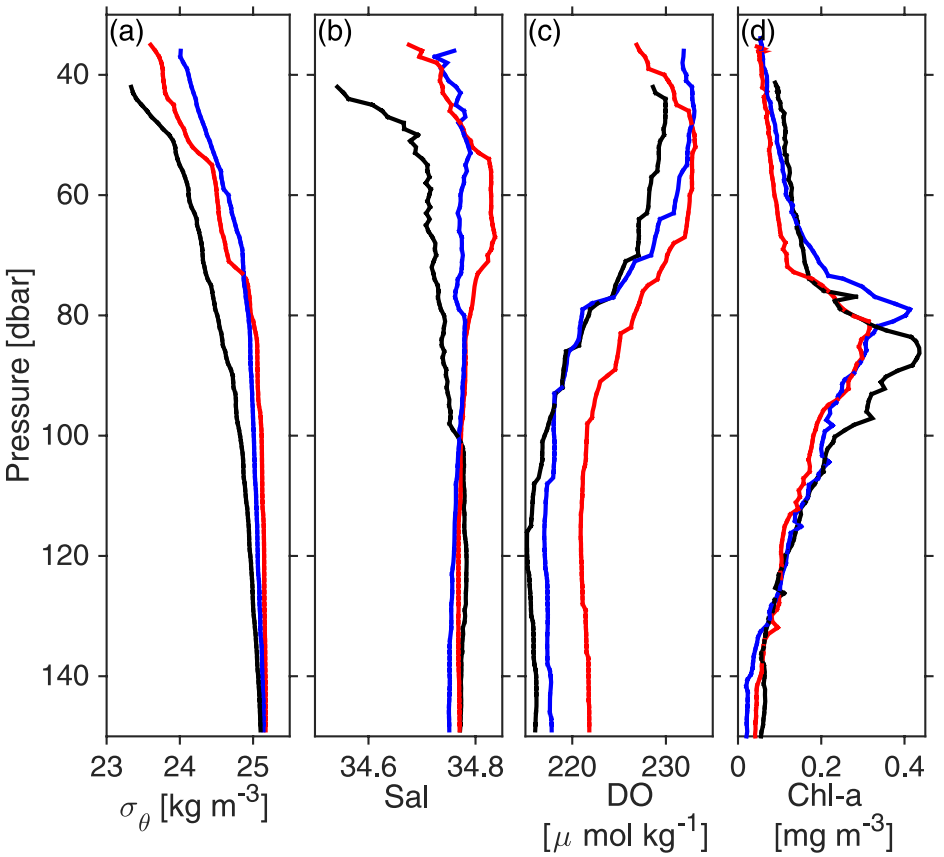

Figure A2. Vertical profiles of (a) sigma theta (σ_θ), (b) salinity (Sal), (c) dissolved oxygen (DO), and (d) chlorophyll *a* (Chl-*a*) from the S1 mooring. The blue line is the profile taken on YDAY 216 at the edge of the cyclonic eddy, black is on YDAY 264 at the transition between two eddies, and the red is on YDAY 285 at the center of the anticyclonic eddy. YDAY, time interval in days since 1 January 2011.

c. Thorpe scale calculation

We calculated the Thorpe scale (Thorpe 1977), L_T, from CTD upcast data because a comparison of the upcast data with the CTD downcast data from the mooring revealed that small eddies induced by the profiler contaminated the calculations during the downcast. We used potential temperature to calculate overturning scales (Alford 2010). To avoid gravitationally stable temperature inversions such as fine-scale intrusions, we also estimated L_T from the potential density and used the smaller of the two L_T values. We defined L_T to be the root mean square of overturning scales over a mixing patch.

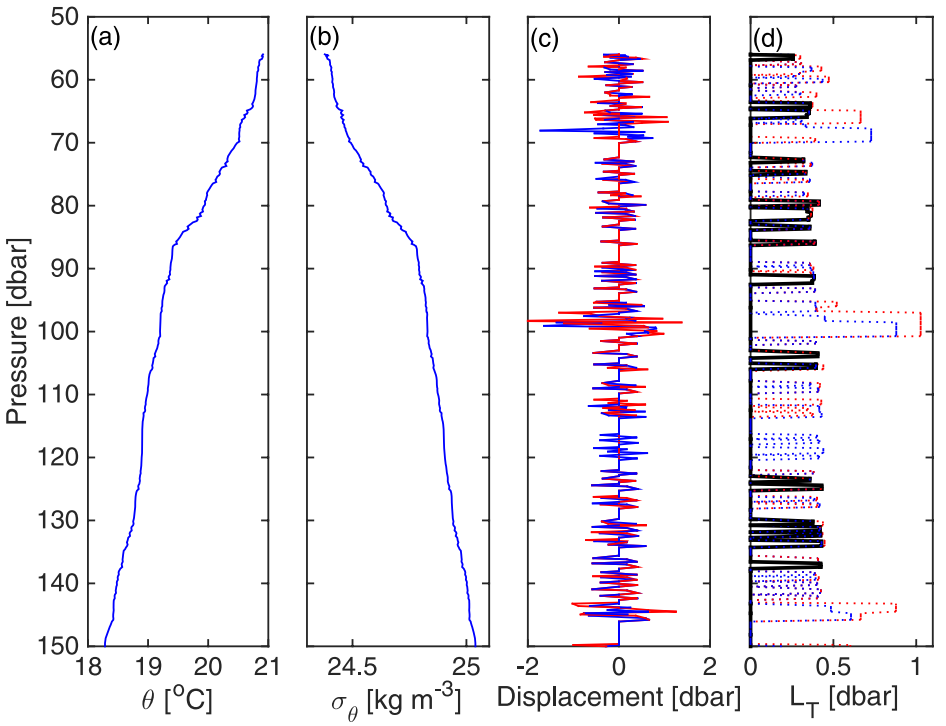

Figure A3. An example of Thorpe scale calculations (YDAY 246): (a) potential temperature (θ), (b) sigma theta (σ_θ), (c) vertical displacements of potential temperature (blue line) and potential density (red line), and (d) Thorpe scales calculated from potential temperature (blue dotted line) and potential density (red dotted line). The thick black line in (d) is the Thorpe scale after removing the possible noise effects. Pressure is used for Thorpe scale calculations. YDAY, time interval in days since 1 January 2011.

The estimation of overturning scales can be affected by noise and the vertical resolution of the CTD (e.g., Alford, Gregg, and Merrifield 2006; Thompson et al. 2007). The error attributable to CTD noise in density (potential temperature), $\Delta\rho = 0.002$ kg m^{-3} ($\Delta\theta = 0.002$°C), which is determined from the accuracy of the sensor, can be determined from $L_{TN} = g\rho^{-1}(2\Delta\rho)N^{-2}$[$L_{TN} = (2\Delta\theta)(\partial\theta/\partial z)^{-1}$ is used when L_T is determined from θ]. Here, g is gravitational acceleration. This L_{TN} was compared with the estimated L_T, and L_T was set to 0 if L_{TN} exceeded L_T. We estimated the buoyancy frequency, N, from reordered potential density data inside mixing patches. Because the CTD resolution was relatively coarse (typically 0.2 m), we could only capture large overturns. We assumed $L_T = 0$ when the mooring did not detect overturns. Figure A3 shows an example of Thorpe scale calculations of overturns on YDAY 246, when, according to the mooring ADCP data (Fig. 15), there was a near-inertial current. This near-inertial current possibly generated

small-scale overturns above 100 dbar. One large overturn of approximately 100 dbar, where stratification was weak, was rejected as instrument noise ($L_{TN} > L_T$) and was not used in further analyses. Finally, it should be noted that, although Thorpe scale distributions seemed to correspond to near-inertial currents (Fig. 15), a further verification has to be made by in situ microstructure measurements to quantify turbulent mixing.

REFERENCES

Alford, M. H. 2010. Sustained, full-water-column observations of internal waves and mixing near Mendocino Escarpment. J. Phys. Oceanogr., *40*, 2643–2660.

Alford, M. H., M. C. Gregg, and M. A. Merrifield. 2006. Structure, propagation, and mixing of energetic baroclinic tides in Mamala Bay, Oahu, Hawaii. J. Phys. Oceanogr., *36*, 997–1018.

Benitez-Nelson, C. R., and D. J. McGillicuddy Jr. 2008. Mesoscale physical-biological-biogeochemical linkages in the open ocean: An introduction to the results of the E-Flux and EDDIES programs. Deep Sea Res., Part II, *55*, 1133–1138.

Bibby, T. S., M. Y. Gorbunov, K. W. Wyman, and P. G. Falkowski. 2008. Photosynthetic community responses to upwelling in mesoscale eddies in the subtropical North Atlantic and Pacific Oceans. Deep Sea Res., Part II, *55*, 1310–1320.

Corno, G., R. M. Letelier, M. R. Abbott, and D. M. Karl. 2008. Temporal and vertical variability in photosynthesis in the North Pacific Subtropical Gyre. Limnol. Oceanogr., *53*, 1252–1265.

D'Asaro, E. A. 1985. The energy flux from the wind to near-inertial motions in the surface mixed layer. J. Phys. Oceanogr., *15*, 1043–1059.

Dillon, T. M. 1982. Vertical overturns: A comparison of Thorpe and Ozmidov length scales. J. Geophys. Res.: Oceans, *87*, 9601–9613.

Ducet, N., P. Y. Le Traon, and G. Reverdin. 2000. Global high-resolution mapping of ocean circulation from the combination of TOPEX/Poseidon and ERS-1 and -2. J. Geophys. Res.: Oceans, *105*, 19477–19498.

Fujiki, T., T. Hosaka, H. Kimoto, T. Ishimaru and T. Saino. 2008. In situ observation of phytoplankton productivity by an underwater profiling buoy system: Use of fast repetition rate fluorometry. Mar. Ecol. Prog. Ser., *353*, 81–88.

Fujiki, T., K. Matsumoto, S. Watanabe, T. Hosaka, and T. Saino. 2011. Phytoplankton productivity in the western subarctic gyre of the North Pacific in early summer 2006. J. Oceanogr., *67*, 295–303.

Gill, A. E. 1984. On the behavior of internal waves in the wakes of storms. J. Phys. Oceanogr., *14*, 1129–1151.

Gordon, R. L. 1996. Acoustic Doppler Current Profiler: Principles of Operation—A Practical Primer, 2nd ed. San Diego, CA: RD Instruments, 52 pp.

Hama, T., T. Miyazaki, Y. Ogaw, T. Iwakuma, M. Takahashi, A. Otsuki, and S. Ichimura. 1983. Measurement of photosynthetic production of a marine phytoplankton population using a stable ^{13}C isotope. Mar. Biol., *73*, 31–36.

Honda, M. C., H. Kawakami, K. Matsumoto, M. Wakita, T. Fujiki, Y. Mino, C. Sukigara, T. Kobari, M. Uchimiya, R. Kaneko, and T. Saino. 2015. Comparison of sinking particles in the upper 200 m between subarctic station K2 and subtropical station S1 based on drifting sediment trap experiments. Special section, J. Oceanogr., *72*, 373–386. doi: 10.1007/s10872-015-0280-x

Honda, M. C., H. Kawakami, S. Watanabe, and T. Saino. 2013. Concentration and vertical flux of Fukushima-derived radiocesium in sinking particles from two sites in the northwestern Pacific Ocean. Biogeosciences, *10*, 3525–3534.

Hosoda, S., T. Ohira, and T. Nakamura. 2008. A monthly mean dataset of global oceanic temperature and salinity derived from Argo float observations. JAMSTEC Rep. Res. Dev., *8*, 47–59.

Inoue, R., and, S. Kouketsu. 2016. Physical oceanographic conditions around the S1 mooring site. Special section, J. Oceanogr., *72*, 453–464. doi: 10.1007/s10872-015-0342-0

Inoue, R., T. Suga, S. Kouketsu, T. Kita, S. Hosoda, T. Kobayashi, K. Sato, H. Nakajima, and T. Kawano. 2016. Western North Pacific Integrated Physical-Biogeochemical Ocean Observation Experiment (INBOX): Part 1. Specifications and chronology of the S1-INBOX floats. J. Mar. Res., *74*(2), 43–69.

Jenkins, W. J. 1988. Nitrate flux into the euphotic zone near Bermuda. Nature, *331*, 521–523.

Jenkins, W. J., and J. C. Goldman. 1985. Seasonal oxygen cycling and primary production in the Sargasso Sea. J. Mar. Res., *43*, 465–491.

Knauer, G. A., J. H. Martin, and K. W. Bruland. 1979. Fluxes of particulate carbon, nitrogen, and phosphorus in the upper water column of the northeast Pacific. Deep-Sea Res., Part A, *26*, 97–108.

Kolber, Z. S., O. Prašil, and P. G. Falkowski. 1998. Measurements of variable chlorophyll fluorescence using fast repetition rate techniques: Defining methodology and experimental protocols. Biochim. Biophys. Acta, Bioenerg. *1367*, 88–106.

Kouketsu, S., R. Inoue, and T. Suga. 2016. Western North Pacific Integrated Physical-Biogeochemical Ocean Observation Experiment (INBOX): Part 3. Mesoscale variability of dissolved oxygen concentrations observed by multiple floats during S1-INBOX. J. Mar. Res., *74*(2), 101–131.

Large, W. G., and S. Pond. 1981. Open ocean momentum flux measurements in moderate to strong winds. J. Phys. Oceanogr., *11*, 324–336.

Lin, I., W. T. Liu, C.-C. Wu, G. T. F. Wong, C. Hu, Z. Chen, W.-D. Liang, Y. Yang, and K.-K. Liu. 2003. New evidence for enhanced ocean primary production triggered by tropical cyclone. Geophys. Res. Lett., *30*, 1718. doi: 10.1029/2003GL017141

Lin, I.-I. 2012. Typhoon-induced phytoplankton blooms and primary productivity increase in the western North Pacific subtropical ocean. J. Geophys. Res.: Oceans, *117*, C03039. doi: 10.1029/2011JC007626

Mackey, M. D., H. W. Higgins, D. J. Mackey, and S. W. Wright. 1997. CHEMTAX User's Manual: A Program for Estimating Class Abundances from Chemical Makers – Application to HPLC Measurements of Phytoplankton Pigments. CSIRO Marine Laboratories Report 229. Hobart, Tasmania, Australia: CSIRO Marine Laboratories.

Mackey, M. D., D. J. Mackey, H. W. Higgins, and S. W. Wright. 1996. CHEMTAX – a program for estimating class abundances from chemical markers: Application to HPLC measurements of phytoplankton. Mar. Ecol. Prog. Ser., *144*, 265–283.

Marañón, E. 2015. Cell size as a key determinant of phytoplankton metabolism and community structure. Annu. Rev. Mar. Sci., *7*, 241–264.

Martiny, A. C., S. Kathuria, and P. M. Berube. 2009. Widespread metabolic potential for nitrite and nitrate assimilation among *Prochlorococcus* ecotypes. Proc. Natl. Acad. Sci. U. S. A., *106*(26), 10787–10792.

McGillicuddy, D. J., Jr., L. A. Anderson, N. R. Bates, T. Bibby, K. O. Buesseler, C. A. Carlson, C. S. Davis, et al. 2007. Eddy/wind interactions stimulate extraordinary mid-ocean plankton blooms. Science, *316*, 1021–1026.

McGillicuddy, D. J., Jr., J. R. Ledwell, and L. A. Anderson. 2008. Response to comment on "Eddy/Wind Interactions Stimulate Extraordinary Mid-Ocean Plankton Blooms." Science, *320*, 448. doi: 10.1126/science.1148974

McGillicuddy, D. J., Jr., A. R. Robinson, D. A. Siegel, H. W. Jannasch, R. Johnson, T. D. Dickey, J. McNeil, A. F. Michaels, and A. H. Knap. 1998. Influence of mesoscale eddies on new production in the Sargasso Sea. Nature, *394*, 263–266.

Michaels, A. F., A. H. Knap, R. L. Dow, K. Gundersen, R. J. Johnson, J. Sorensen, A. Close, et al. 1994. Seasonal patterns of ocean biogeochemistry at the U.S. JGOFS Bermuda Atlantic Time-series Study site. Deep Sea Res., Part I, *41*, 1013–1038.

Pollard, R. T., and R. C. Millard Jr. 1970. Comparison between observed and simulated wind-generated inertial oscillations. Deep-Sea Res. Oceanogr. Abstr., *17*, 813–816, IN5, 817–821.

Price, J. F. 1981. Upper ocean response to a hurricane. J. Phys. Oceanogr., *11*, 153–175.

Price, J. F. 1983. Internal wave wake of a moving storm. Part I: Scales, energy budget and observations. J. Phys. Oceanogr., *13*, 949–965.

Price, J. F., T. B. Sanford, and G. Z. Forristall. 1994. Forced stage response to a moving hurricane. J. Phys. Oceanogr., *24*, 233–260.

Qiu, B., P. Hacker, S. Chen, K. A. Donohue, D. R. Watts, H. Mitsudera, N. G. Hogg, and S. R. Jayne. 2006. Observations of the subtropical mode water evolution from the Kuroshio Extension System Study. J. Phys. Oceanogr., *36*, 457–473.

Raven, J. A. 1998. The twelfth Tansley lecture. Small is beautiful: The picophytoplankton. Funct. Ecol., *12*, 503–513.

Redfield, A. C., B. H. Ketchum, and F. A. Richards. 1963. The influence of organisms on the composition of sea-water, *in* The Sea, Vol. 2, The Composition of Sea-Water: Comparative and Descriptive Oceanography, M. N. Hill, ed. New York: Wiley-Interscience, 26–77.

Saito, K. 2012. The JMA nonhydrostatic model and its application to operation and research, *in* Atmospheric Model Applications, I. Yucel, ed. Rijeka, Croatia: InTech, 85–110.

Saito, K., T. Fujita, Y. Yamada, J.-I. Ishida, Y. Kumagi, K. Aranami, S. Ohmori, et al. 2006. The operational JMA nonhydrostatic mesoscale model. Mon. Weather Rev., *134*, 1266–1298.

Sanford, T. B., J. F. Price, and J. B. Girton. 2011. Upper-ocean response to Hurricane Frances (2004) observed by profiling EM-APEX floats. J. Phys. Oceanogr., *41*, 1041–1056.

Shibano, R., Y. Yamanaka, N. Okada, T. Chuda, S. Suzuki, H. Niino, and M. Toratani. 2011. Responses of marine ecosystem to typhoon passages in the western subtropical North Pacific. Geophys. Res. Lett., *38*, LI8608. doi: 10.1029/2011gl048717

Spitzer, W. S., and W. J. Jenkins. 1989. Rates of vertical mixing, gas exchange and new production: Estimates from seasonal gas cycles in the upper ocean near Bermuda. J. Mar. Res., *47*, 169–196.

Suggett, D. J., S. C. Maberly, and R. J. Geider. 2006. Gross photosynthesis and lake community metabolism during the spring phytoplankton bloom. Limnol. Oceanogr., *51*, 2064–2076.

Sukigara, C., T. Suga, T. Saino, K. Toyama, D. Yanagimoto, K. Hanawa, and N. Shikama. 2011. Biogeochemical evidence of large diapycnal diffusivity associated with the subtropical mode water of the North Pacific. J. Oceanogr., *67*, 77–85.

Suzuki, R., and T. Ishimaru. 1990. An improved method for the determination of phytoplankton chlorophyll using N, N-dimethylformamide. J. Oceanogr. Soc. Jpn., *46*, 190–194.

Thompson, A. F., S. T. Gille, J. A. MacKinnon, and J. Sprintall. 2007. Spatial and temporal patterns of small-scale mixing in Drake Passage. J. Phys. Oceanogr., *37*, 572–592.

Thorpe, S. A. 1977. Turbulence and mixing in a Scottish loch. Philos. Trans. R. Soc. London, 286*A*, 125–181.

Weller, R. A. 1982. The relation of near-inertial motions observed in the mixed layer during the JASIN (1978) experiment to the local wind stress and to the quasi-geostrophic flow field. J. Phys. Oceanogr., *12*, 1122–1136.

Welschmeyer, N. A. 1994. Fluorometric analysis of chlorophyll a in the presence of chlorophyll b and pheopigments. Limnol. Oceanogr., *39*, 1985–1992.

Zapata, M., F. Rodríguez, and J. L. Garrido. 2000. Separation of chlorophylls and carotenoids from marine phytoplankton: A new HPLC method using a reversed phase C_8 column and pyridine-containing mobile phases. Mar. Ecol. Prog. Ser., *195*, 29–45.

Zhao, H., J. Shao, G. Han, D. Yang, and J. Lv. 2015. Influence of Typhoon Matsa on phytoplankton chlorophyll-*a* off East China. *PLoS ONE*, 10(9), e0137863. doi: 10.1371/journal.pone.0137863

Received: *14 November 2013*; revised: *18 March 2016*.